Hindawi
Mathematical Problems in Engineering
Volume 2017, Article ID 5670697, 11 pages
https://doi.org/10.1155/2017/5670697

Research Article

Error Correction of Measured Unstructured Road Profiles Based on Accelerometer and Gyroscope Data

Jinhua Han, Xiaoqiang Yang, Huanliang Li, and Hongxin Cui

Engineering Institute, PLA University of Science and Technology, Nanjing 210007, China

Correspondence should be addressed to Xiaoqiang Yang; 3113593699@qq.com

Received 25 October 2016; Accepted 27 December 2016; Published 24 January 2017

Academic Editor: Francesco Franco

This paper describes a noncontact acquisition system composed of several time synchronized laser height sensors, accelerometers, gyroscope, and so forth in order to collect the road profiles of vehicle riding on the unstructured roads. A method of correcting road profiles based on the accelerometer and gyroscope data is proposed to eliminate the adverse impacts of vehicle vibration and attitudes change. Because the power spectral density (PSD) of gyro attitudes concentrates in the low frequency band, a method called frequency division is presented to divide the road profiles into two parts: high frequency part and low frequency part. The vibration error of road profiles is corrected by displacement data obtained through two times integration of measured acceleration data. After building the mathematical model between gyro attitudes and road profiles, the gyro attitudes signals are separated from low frequency road profile by the method of sliding block overlap based on correlation analysis. The accuracy and limitations of the system have been analyzed, and its validity has been verified by implementing the system on wheeled equipment for road profiles' measuring of vehicle testing ground. The paper offers an accurate and practical approach to obtaining unstructured road profiles for road simulation test.

1. Introduction

Road profile is the most important external excitation of the ground vehicle, which influences vehicle ride comfort, operational stability, driving reliability, fatigue life of components, and so forth [1–3]. Therefore, providing accurate road profile for vehicle reliability testing and simulation has been an important research content in this field.

The actual roads can be divided into structured and unstructured roads. The structured roads generally refer to the well-structured pavements with flat road surface and regular edge such as the expressway and urban roads. The unstructured roads generally refer to the less structured roads with high roughness, including the nonpaved roads such as gravel road and sand road, "bad road" whose road degree is E or below E and road cover is damaged, roadless road, and strengthened test pavement. Currently, road profile measuring concentrates on the structured roads mainly measured by the Highway Department. Moreover, lots of structured road profile models have been built up and can be simulated and reconstructed accurately [4, 5]. However, with regard to the unstructured roads, there is no standardized road profile to utilize because of the potential complexity. Furthermore, the unstructured road profile has evident non-Gaussian characteristics largely due to a large number of high amplitude excitations [6]. The characterization of the structured road profile based on the assumption of stationary, random, and Gaussian is difficult to be applied to the unstructured roads [7]. Therefore, an in situ acquisition operation of unstructured roads is always needed before performing any road simulation.

Since the 1960s a lot of studies had been done for measuring road profiles, and many kinds of measuring devices had been invented [8–11], which contain Level and Rod, Multiwheel Profilograph, BPR Roughometer, Inertial Profiler, Laser Profiler, and so forth. But they are always difficult to simultaneously consider the measuring speed and accuracy. Nowadays, the most commonly used noncontact profilometers can measure the road profile with pretty high accuracy [12, 13]. Nonetheless, this system may not be applicable for the unstructured road profile measuring due to the following reasons [14]. The road profile mainly

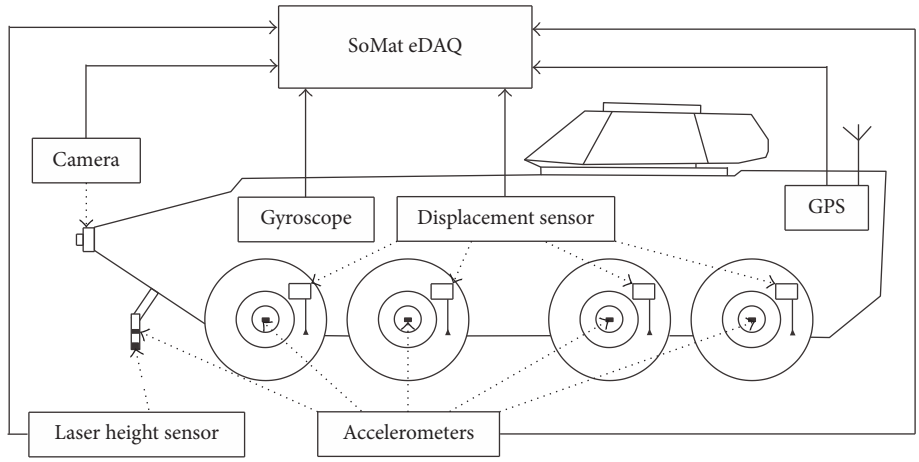

Figure 1: Road profile acquisition system of the vehicle.

depends on the relative displacement between the sensor and the road surface measured by the sensor (laser, infrared, or ultrasonic) mounted on the vehicle. The obtained final displacement could represent the road profile only when the vehicle is not excessively interrupted and maintains steady while driving through the road. Obviously, this hypothesis is not true for unstructured roads because of the bumpiness of the unstructured road which result in severe vibration and attitudes' change of the vehicle and the major variation in the vehicle speed [15, 16].

To solve the problem, a laser measuring system for the unstructured road is proposed to realize the fast measurement of the road profiles, vibration acceleration, and gyro attitudes of the vehicle. To improve the accuracy of the measured road profiles, an error correction method based on measured acceleration and gyro attitudes data is discussed in detail. Aiming at the characteristic that the PSD of vehicle attitudes concentrates in the low frequency band, the measured road profile can be divided into high frequency part and low frequency part by the method of frequency division. Then the vibration error of the measured road profile is corrected by displacement data obtained through two times integration of measured acceleration data. The attitude error of the measured road profile is corrected by signal separation based on sliding block overlap and correlation analysis. The proposed acquisition system has been used in the unstructured road profile measurement of vehicle testing ground, and its validity has been evaluated in the paper.

2. Laser Road Profile Acquisition System

For the reliability simulation of the vehicle, the 2D profile curve in the direction of the vehicle wheels' orbit is generally used as the research object. A road profile acquisition system is shown in Figure 1 which integrates the gyro attitudes, GPS, vibration acceleration, and displacement measuring. The system can be used to measure road profiles of structured roads (asphalt road, expressway, etc.) and unstructured roads (gravel road, cross-country path, strengthen-road, etc.). The test vehicle is an 8×8 wheeled vehicle with independent suspension [17], which could reduce the impact of the road profiles to the vehicle and improve ride comfort. However, the vehicle's attitude change is inevitable when driving on the unstructured roads. Generally, the frequencies of sensors are high enough for the acquisition. The sampling frequencies of acceleration and road profile data are 1 kHz, while the sampling frequency of gyro attitudes is 200 Hz.

The road profile acquisition system consists of a HBM SoMat eDAQ System (data acquisition and record), a RMS Strapdown Platform System (mounted in the center of the vehicle and measuring vehicle's attitudes change), two groups of Datron HF-500C laser height sensors (measuring the relative displacement between sensor and road surface, i.e., the road profile), ten groups of ENDEVCO 7596 accelerometers (measuring the vibration acceleration of laser sensors and the spindles of the vehicle), some groups of cable displacement sensors (measuring displacement of the spindles), an ordinary GPS module (measuring the longitude, latitude, altitude, and speed of the vehicle), an AXIS P1311 webcam (recording video information of testing roads), and so forth. As shown in Figure 2, the laser height sensors and accelerometers are counted on the brackets that are fixed on both sides of the front of the vehicle.

3. Error Correction of Road Profiles

The road profile includes the large-scale signal that is from low frequency to high frequency; the laser height sensor could barely measure the signals of all frequency bands. In addition, the devices of the acquisition system are fixed on the vehicle; the road profiles measured by laser sensors are mostly high frequency and short wavelength signals (the wavelength is less than the wheelbase of testing vehicle). Therefore, the measuring frequency band is divided into several sections. For the low frequency and long wavelength part of road profile that the laser sensor cannot measure (the frequency is generally lower than 0.1 Hz), a Global Positioning System

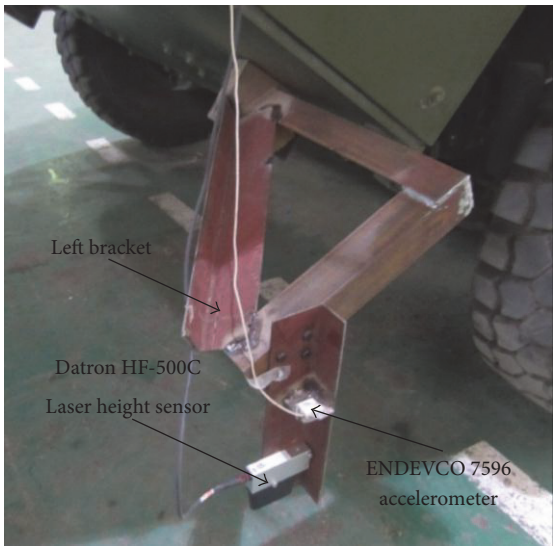

Figure 2: The mounted sensors of the acquisition system (left bracket).

(GPS) receiver supplemented with Real Time Kinematics (RTK) technology can easily measure the road profile with centimeter level accuracy and has been widely used in road profile measurement [18, 19].

For the short wavelength signals above 0.1 Hz that the laser sensor can measure, they are also divided into two parts due to the PSD of the vehicle attitudes [20]. To correct the errors of road profile caused by the vibration and attitudes change of the testing vehicle, the vibration acceleration and gyro attitudes are measured. For the road profile with frequency below 3 Hz (0.1 Hz~3 Hz), the error is corrected by the measured gyro attitudes. For the road profile with frequency above 3 Hz (>3 Hz), the error is corrected by displacement data obtained by two times integration of measured acceleration data. Finally, the final corrected road profile is obtained by combining the corrected low frequency part and the corrected high frequency part; its specific calculation process is shown in Figure 3. Each filtering frequency can be adjusted according to the actual need in the calculation process.

3.1. Division Frequency Determined. The division frequency of measured road profiles is mainly determined by the gyro attitudes frequency band and the road frequency band. The road frequency band depends on vehicle forward speed v and the wavelengths of road profile. The wavelengths of road profile are mainly concentrated within a certain range. It is hypothesized that λ_1 and λ_2 are the lower and upper of the wavelengths, respectively. Then the frequencies of road wavelengths measured by the laser sensor can be expressed as

$$f_L = \frac{v}{\lambda_2}, \qquad f_H = \frac{v}{\lambda_1}. \tag{1}$$

Therefore, to divide the gyro attitudes frequency and road frequency of measured road profile, the division frequency f_d should be lower than the road frequency band $[f_L, f_H]$ and higher than the gyro attitudes frequency band $[f_a, f_b]$, which can be expressed as

$$f_b < f_d < f_L = \frac{v}{\lambda_2}. \tag{2}$$

3.2. Acceleration Integration. To correct the vibration error due to the movement of laser sensor along with the testing vehicle, the displacement is calculated by two times integration of measured acceleration data.

As shown in Figure 4, the measured acceleration signal should be preprocessed first, including singularity removed & detrend and band-pass filtering in order to improve measuring accuracy. Then the vibration velocity is obtained by acceleration integration. Finally, the vibration displacement is obtained by velocity integration after band-pass filtering. Scilicet, the vibration displacement is the vibration error of road profile. Therefore, the vibration error of road profile can be corrected by subtracting the vibration displacement.

3.3. Mathematics Description of Gyro Attitude. To realize the error correction of measured road profile due to the vehicle's attitudes change, the mathematical model between vehicle's attitudes and road profile should be established first after analyzing the relation between them. Due to the relativity of motion, the corresponding coordinate system should be introduced in the gyro attitudes measurement. The gyro attitudes measured by strapdown gyroscope in this paper are the geometric angles of the body coordinate system (BCS) $ox_by_bz_b$ relative to the geographic coordinate system (GCS) $ox_ty_tz_t$. The BCS $ox_by_bz_b$ denotes the coordinate system fixed on the testing vehicle that its origin is located at the center of the vehicle, ox_b points to forward along the longitudinal axis of the vehicle, oy_b points to left along the horizontal axis of the vehicle, and oz_b is perpendicular to the ox_by_b plane and points to up along the vertical axis of the vehicle. The GCS $ox_ty_tz_t$ denotes the coordinate system that its origin is also located at the center of the vehicle, ox_t points to east, oy_t points to north, and oz_t points to sky along the vertical direction according to the right-hand rule.

The gyro attitudes of the testing vehicle include three parameters [21], yaw angle γ, pitch angle θ, and roll angle φ. They denote the rotation angle of the vector around the x, y, and z axes, respectively. According to the right-hand rule, the inverse rotation is clockwise.

As shown in Figure 5, in the case of the invariant of the coordinate origin, the GCS $ox_ty_tz_t$ is used as the reference coordinate system. Then the BCS $ox_by_bz_b$ is obtained after triple rotation according to the order of $z - y - x$. Its specific conversion process is as follows:

$$ox_ty_tz_t \xrightarrow[oz_t]{\gamma} ox'y'z_t \xrightarrow[oy']{\theta} ox_by'z' \xrightarrow[ox_b]{\varphi} ox_by_bz_b. \tag{3}$$

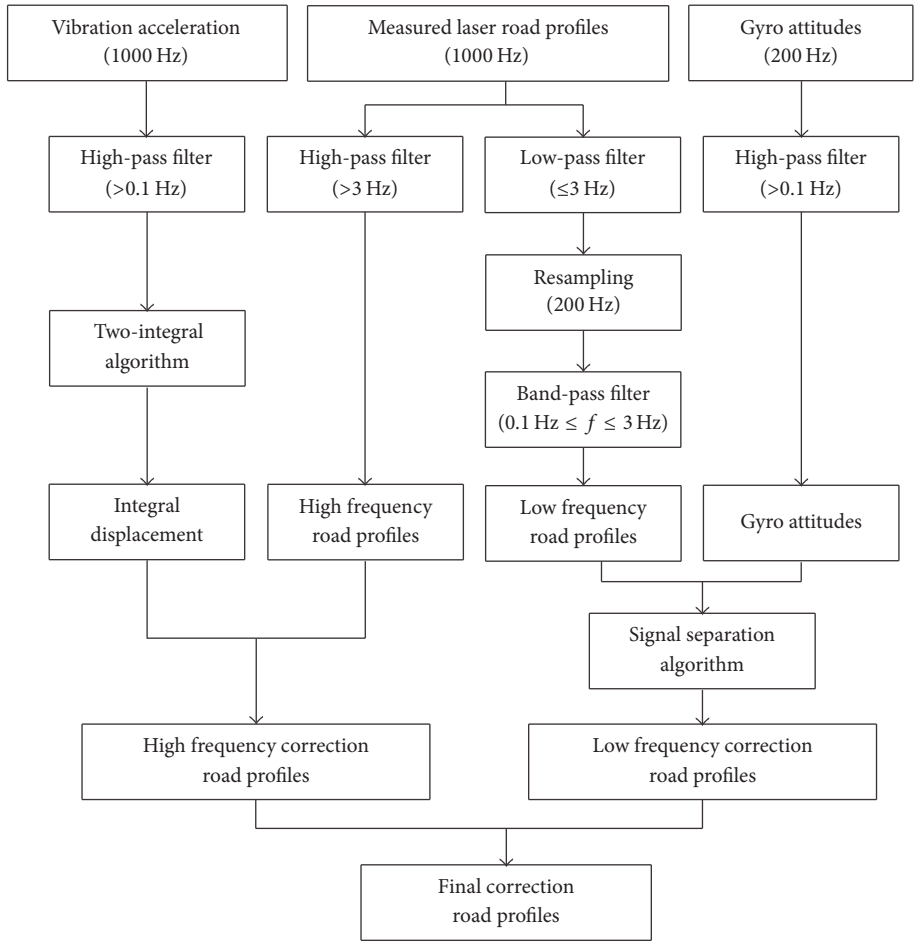

Figure 3: The calculation flow chart of correcting road profile.

Then the transformation relation from the BCS $ox_by_bz_b$ to the GCS $ox_ty_tz_t$ is shown as follows:

$$\begin{bmatrix} x_t \\ y_t \\ z_t \end{bmatrix} = \mathbf{C}_b^t \begin{bmatrix} x_b \\ y_b \\ z_b \end{bmatrix}, \tag{4}$$

where $[x_t \quad y_t \quad z_t]^T$ and $[x_b \quad y_b \quad z_b]^T$ denote the coordinate of the laser sensor in the GCS $ox_ty_tz_t$ and the BCS $ox_by_bz_b$, respectively. $\mathbf{C}_b^t$ denotes the rotational transformation matrix, also called the strapdown matrix.

The emphasis of realizing the sensor coordinate transformation between different coordinate systems is the solution of the strapdown matrix $\mathbf{C}_b^t$. Therefore, the obtained strapdown matrix $\mathbf{C}_b^t$ according to the order of $z - y - x$ can be expressed as

$$\begin{aligned} \mathbf{C}_b^t = \mathbf{C}_{z,\gamma}\mathbf{C}_{y,\theta}\mathbf{C}_{x,\varphi} &= \begin{bmatrix} \cos\gamma & -\sin\gamma & 0 \\ \sin\gamma & \cos\gamma & 0 \\ 0 & 0 & 1 \end{bmatrix} \begin{bmatrix} \cos\theta & 0 & \sin\theta \\ 0 & 1 & 0 \\ -\sin\theta & 0 & \cos\theta \end{bmatrix} \begin{bmatrix} 1 & 0 & 0 \\ 0 & \cos\varphi & -\sin\varphi \\ 0 & \sin\varphi & \cos\varphi \end{bmatrix} \\ &= \begin{bmatrix} \cos\theta\cos\gamma & \sin\varphi\sin\theta\cos\gamma - \cos\varphi\sin\gamma & \cos\varphi\sin\theta\cos\gamma + \sin\varphi\sin\gamma \\ \cos\theta\sin\gamma & \sin\varphi\sin\theta\sin\gamma + \cos\varphi\cos\gamma & \cos\varphi\sin\theta\sin\gamma - \sin\varphi\cos\gamma \\ -\sin\theta & \sin\varphi\cos\theta & \cos\varphi\cos\theta \end{bmatrix}, \end{aligned} \tag{5}$$

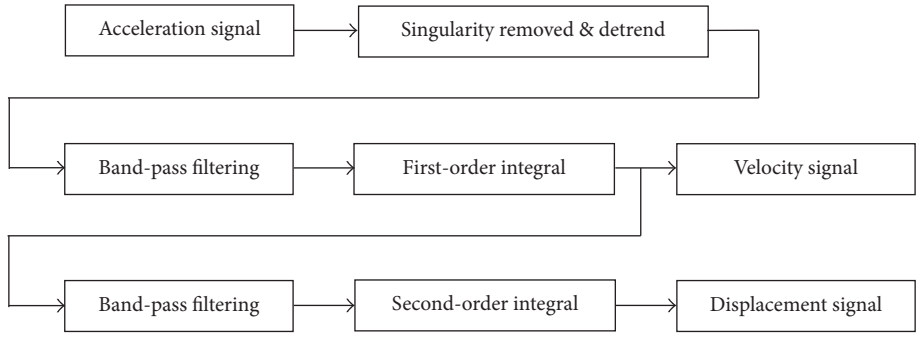

Figure 4: The flow chart of acceleration integration.

where $\mathbf{C}_{z,\gamma}$ denotes the rotational transformation matrix around the z-axis with rotation angle γ. $\mathbf{C}_{y,\theta}$ denotes the rotational transformation matrix around the y-axis with rotation angle θ. $\mathbf{C}_{x,\varphi}$ denotes the rotational transformation matrix around the x-axis with rotation angle φ.

The research of road profile is concerned with the road roughness that is perpendicular to the ground. Scilicet, the main external excitation of the testing vehicle is the displacement of the road in the z-axis direction along the direction of the vehicle, rather than in the x-axis or y-axis direction. Thus, substituting (5) into (4) can be expressed as

$$z_t = \begin{bmatrix} -\sin\theta & \sin\varphi\cos\theta & \cos\varphi\cos\theta \end{bmatrix} \begin{bmatrix} x_b \\ y_b \\ z_b \end{bmatrix}. \quad (6)$$

When the change of the gyro attitudes angles φ, θ, and γ is small, (6) can be simplified as

$$z_t = -\theta \cdot x_b + \varphi \cdot y_b + z_b. \quad (7)$$

Thus, the error of measured road profile caused by the gyro attitudes is given by

$$\Delta z = z_t - z_b = -\theta \cdot x_b + \varphi \cdot y_b. \quad (8)$$

As shown in (8), the measured road profiles are mainly affected by the pitch angle θ and roll angle φ; the yaw angle γ has almost no influence on them. Due to the relatively large values of x_b and y_b (up to several meters), the small changes of vehicle's attitudes can cause large error of the measured road profiles. Therefore, the error of measured road profiles caused by vehicle's attitudes must be corrected based on the calculation result of (8).

3.4. Error Correction Based on Signal Separation. According to (8), the relation between the vehicle's attitudes and the error of road profile Δz can be approximately regarded as linear. Hence, the measured road profile can be regarded as the linear mixture of true road and vehicle's attitude signals. The error correction of measured road profile due to vehicle's attitudes change can be regarded as the signal separation of mixed signal [22]. The mixed and separation process of

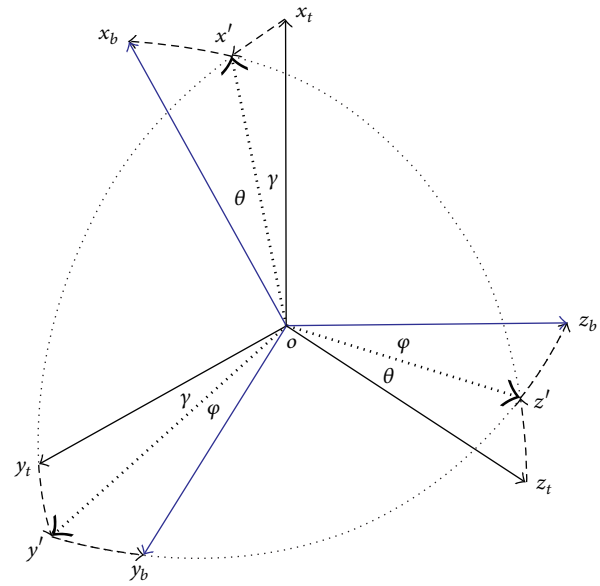

Figure 5: Coordinate transformation diagram.

measured road profiles is shown in Figure 6. x_1 denotes the true road profile, that is, unseparated signal. The additive mixed signal $y = x_1 + x_2$ measured by the laser height sensor T_1 consists of signals x_1 and x_2 that are obtained through the unknown transmission channel H_1. $\tilde{x}_2$ denotes the vehicle's attitudes measured by gyroscope T_2 located in the center of the vehicle. Then the mixed signal y is separated to obtain the accurate road profile based on the observed signal y and the reference signal $\tilde{x}_2$.

The signal separation algorithm in this paper is based on the assumption of linear mixture. However, the signal mixing has a certain nonlinearity in fact. To satisfy the assumption of linear mixture as much as possible, a method called sliding block overlap is proposed to correct the low frequency road profile. The correction steps are shown as follows.

Step 1 (signals acquisition). The low frequency road profile y and vehicle's attitudes (pitch angle θ, roll angle φ, and yaw angle γ) are measured and calculated first. Then, according to (8), the reference signal $\tilde{x}_2 = -\theta \cdot x_b + \varphi \cdot y_b$ is obtained.

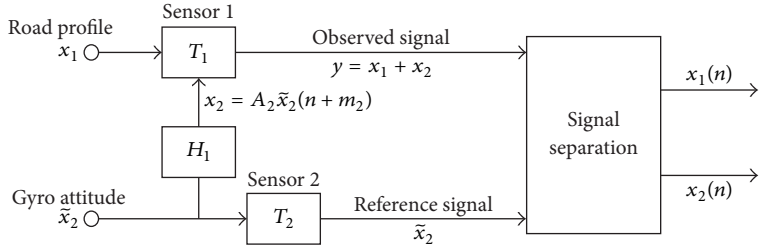

Figure 6: The mixed and separation process of measured road profiles.

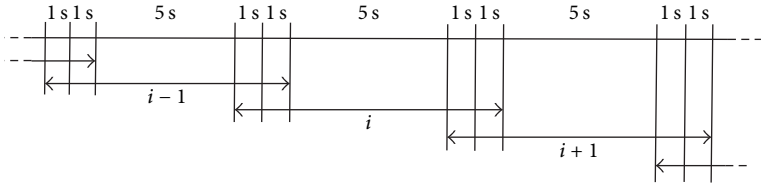

Figure 7: The schematic diagram of the data segmentation.

Step 2 (estimation of the time shift m_2 by cross-correlation function). The cross-correlation function is a description of the correlation between random signal $\tilde{x}_2$ and y at different time. According to the properties of the cross-correlation function, when $R_{y\tilde{x}_2}(\tau)$ takes the maximum value at $\tau = \tau_1$, the time shift $m_2 = \tau_1$ of the signals is determined.

Step 3 (signal sliding segmentation and overlap). The schematic diagram of the data segmentation is shown in Figure 7. The testing data of the time length T is divided into N segments of the equal length t_1. Then there are $N - 1$ overlapping segments of the equal length t_2. Data segment number N and length t can be adjusted according to the actual situation in order to achieve the best effect. The relation of the parameters is shown by

$$N \cdot t_1 + (N - 1) \cdot t_2 = T. \tag{9}$$

After completing the time shift of Step 2, the signal sliding segmentation and overlap of measured road profile y and reference attitudes $\tilde{x}_2$ are accomplished according to the above method. Then the i segment of measured road profile y and reference attitudes $\tilde{x}_2$ are recorded as y_i and $\tilde{x}_{2i}$, respectively.

Step 4 (amplitude adjustment). The amplitude of the vehicle's attitude signal will change during the process of mixing into the road profile. Therefore, the amplitude adjustment is required to keep the reference signal $\tilde{x}_2$ in the same amplitude as the mixed signal y. To reduce the nonlinearity error, amplitude adjustment is performed for each data segment. The amplitude of reference signal $\tilde{x}_{2i}$ after amplitude adjustment can be computed as

$$A'_{xi} = (A_{xi} - m_{xi}) \frac{d_{yi}}{d_{xi}} + m_{xi}, \tag{10}$$

where A_{xi} denotes the amplitudes of references signal $\tilde{x}_{2i}$. m_{xi} denotes the mean values of references signal $\tilde{x}_{2i}$. d_{xi} and d_{yi} denote the mean square errors (MSE) of references signal $\tilde{x}_{2i}$ and mixed signal y_i, respectively. Then the adjusted reference signal $\tilde{x}'_{2i}$ has the same amplitude and distribution as the mixed signal y_i.

Step 5 (segment error correction). The true road profile x_{1i} can be computed from

$$x_{1i} = y_i - \tilde{x}'_{2i}. \tag{11}$$

Step 6 (smooth connection of segmental data). The corrected segmented road profile is connected in a time sequence. For the data overlap part, the arithmetic mean is applied to reduce the difference within the data connection. Moreover, for the data connection, adaptive correction method based on local signal baseline adjustment is used to realize smooth connection of segmental data [23]. Then the low frequency road profile is corrected and obtained by the above steps.

Step 7 (signal merging). After correcting the low frequency and high frequency road profile, the final corrected road profile is obtained by combining the low frequency and high frequency corrected road profile.

4. Application

By using the acquisition system shown in Figure 1, all road signals had been acquired during the testing vehicle riding through the unstructured proving ground (PG) roads of Beijing vehicle testing ground, which include Ripple Tracks, Belgian Road, Cobblestone Tracks, Washboards, Body Twist Lane, and Potholes Road. The original collected signals mainly include road profiles (with frequency of 1 kHz), vibration acceleration (with frequency of 1 kHz), and gyro attitudes (with frequency of 200 Hz). Then some preprocessing methods including the identification and correction of abnormal errors, the extraction of signal trends, and digital filtering are implemented to the original collected signals

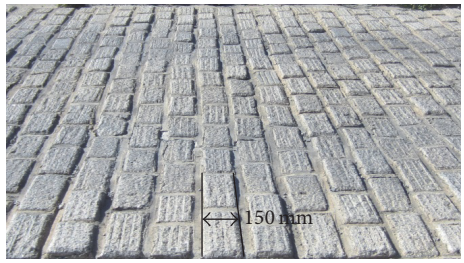

Figure 8: The Belgian Road in picture.

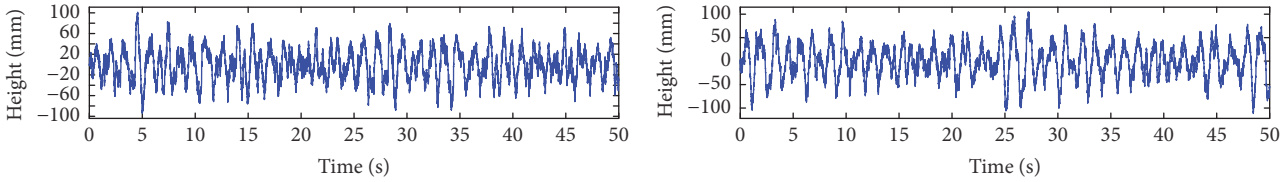

Figure 9: Measured road profiles of Belgian Road. (a) The left wheel; (b) the right wheel.

[24]. The Belgian Road is a typical unstructured road and man-made test road whose characteristics are determined. When driving on the Belgian Road, the testing vehicle bumps violently, which can cause random vibration of rolling, pitching, and vertical direction. Therefore, the Belgian Road is expressed as an example to verify the validity and accuracy of the error correction algorithm mentioned above in this paper. The average vehicle speed is about 18.5 km/h (5.14 m/s) during the testing. Figure 8 shows the Belgian Road in picture. The average length of the cobbles in the direction of testing vehicle travel is about 150 mm. Figure 9 gives the road profiles corresponding to two wheels measured by laser height sensors. Figure 10 presents the vehicle's attitudes measured by strapdown gyroscope.

4.1. Frequency Division of Measured Road Profiles. As mentioned above, the vehicle's attitudes mainly affect the low frequency band of measured road profiles which is about 0.1 Hz~2.0 Hz. Therefore, the road profile is divided into high frequency part (>3 Hz) and low frequency part (0.1 Hz~3 Hz) by frequency division. As shown in Figure 11 is the high frequency and low frequency road profile of right wheel.

4.2. Acceleration Integration. As shown in Figure 12, the integral velocity and displacement signal are obtained by acceleration integration measured by accelerometer fixed on the right bracket (Figure 2). The error of measured road profile caused by vehicle vibration is mainly concentrated in ±0.5 mm (except for the individual), and the impact is about 2%. Due to the relative displacement between the sensor and the road surface measured by laser height sensor, the corrected high frequency road profile can be computed by subtracting integral displacement from the original high frequency road profile. Thus the impact of vehicle vibration to road profile acquisition is removed.

Table 1: Correlation coefficients between road profiles and gyro attitudes.

Correlation coefficients	Roll φ	Pitch θ	Yaw γ
Original signal ($f > 0.1$ Hz)			
Left road profile	−0.4518	0.7421	0.1886
Right road profile	0.5677	0.7943	0.1933
High frequency signal ($f > 3$ Hz)			
Left road profile	0.0610	0.0037	−0.0114
Right road profile	−0.0531	0.0069	0.0184
Low frequency signal (0.1 Hz $\le f \le$ 3 Hz)			
Left road profile	−0.4905	0.7765	0.2169
Right road profile	0.5919	0.8201	0.2181

4.3. Correlation Analysis. As mentioned previously, the gyro attitudes have great influence on the road profile measuring. However, the impacts of yaw angle γ, pitch angle θ, and roll angle φ on the road profile measuring are different. Generally, the impact size between gyro attitudes and road profile can be analyzed by correlation coefficient ρ_{XY}. The correlation coefficient ρ_{XY} between signals X and Y is between −1 and 1. When $\rho_{XY} = 0$, X and Y are not related. When $|\rho_{XY}| = 1$, X and Y are completely related. When $|\rho_{XY}| > 0.8$, X and Y are highly related. When $|\rho_{XY}| < 0.3$, X and Y are lowly related. When $0.3 \le |\rho_{XY}| \le 0.8$, X and Y are moderately related. The greater the absolute value of ρ_{XY}, the higher the correlation between X and Y.

To analyze the relation between measured road profile and gyro attitudes, the correlation coefficients between them are computed and shown in Table 1. The pitch angle θ and roll angle φ have a high correlation with the measured

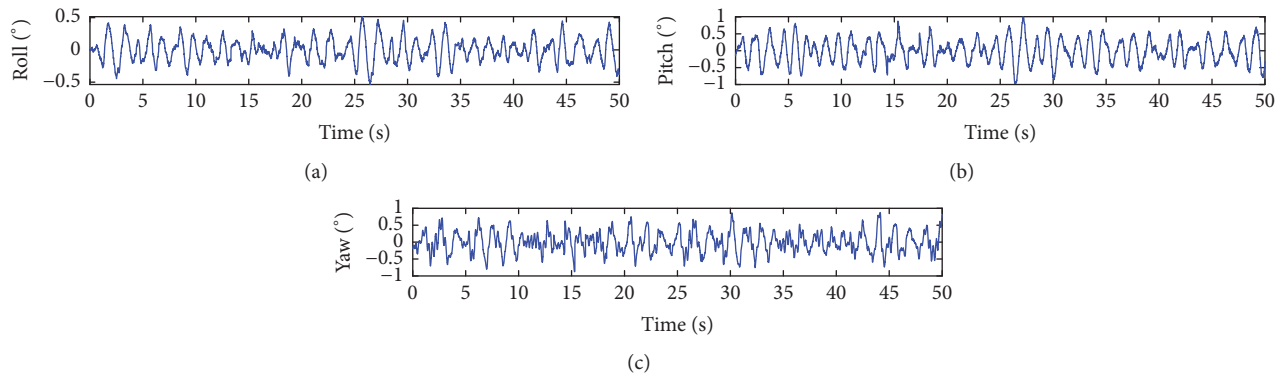

Figure 10: Measured vehicle's attitudes of Belgian Road. (a) The roll angle; (b) the pitch angle; and (c) the yaw angle.

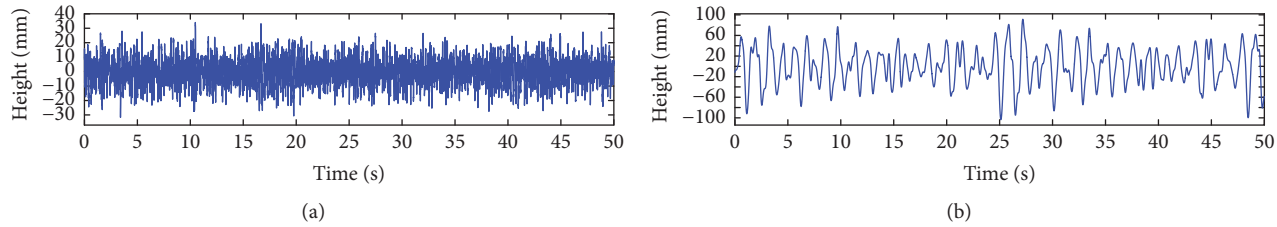

Figure 11: Road profile after frequency division (right wheel). (a) The high frequency part; (b) the low frequency part.

road profile, which verifies the validity of (8). Besides, the correlation coefficients between gyro attitudes and high frequency road profile are close to zero. This means that they are basically not related. The impact of vehicle's attitudes on road profile measuring is mainly concentrated in the low frequency band (≤3 Hz), which verifies the feasibility of the frequency division method. Therefore, the impact of vehicle's attitudes to road profile acquisition can be removed only by correcting the low frequency road profile.

4.4. Error Correction. As shown in Figure 2, the laser height sensor and accelerometer are fixed on the bracket in front of the testing vehicle. The distances from the sensors to the vehicle center in each direction are $x = 4500$ mm, $y = 1300$ mm, and $z = 1050$ mm. The curves of low frequency road profile and pitch angle θ are shown in Figure 13. According to the comparison, the low frequency road profile and pitch angle θ have the same change trend, which means high correlation between them.

Known from Section 3 of the paper, the error of vehicle's attitudes to measured road profile Δz is computed as (8). Then the error correction is completed according to the steps mentioned in Section 3.4. The corrected low frequency road profile is explicitly shown in Figure 14. The large wave of road profile caused by vehicle's attitudes is well removed. Then the final corrected road profile is obtained by combining low frequency road profile after removing attitudes' impact and high frequency road profile after removing vibration impact, as shown in Figure 15. The amplitude of road profile decreases from about 50 mm to 20 mm, which is more consistent with the real road features of the Belgian Road in vehicle testing ground.

Table 2: RMS comparison of road profile before and after correction.

Road profile	RMS (mm)	
	Original	Corrected
High frequency	9.2798	9.2793
Low frequency	35.3676	15.0620
Final	36.1104	18.2179

For comparison, the Root Mean Square (RMS) of the road profiles before and after error correction are calculated and shown in Table 2. By the error correction method raised in this paper, the RMS of road profile reduces from 36.1104 mm to 18.2179 mm. Obviously, the validity of the error correction method can be verified easily by comparing Figures 9 and 15.

To further analyze the validity of the error correction method proposed in the paper, the space road spectrum is introduced for comparison. According to standard ISO/DIS 8608 and GB/T 7031-2005, the model and grading method based on the PSD of the road roughness were worked out. The fitting expression of the road PSD using power function can be shown as

$$G_d(n) = G_d(n_0)\left(\frac{n}{n_0}\right)^{-W}, \tag{12}$$

where n denotes the space frequency in m^{-1}. $n_0 = 0.1\,\mathrm{m}^{-1}$ denotes the reference space frequency. $G_d(n_0)$ denotes the road roughness coefficient, which is the value of PSD at n_0 in m^3. W denotes the frequency index (the general value is 2).

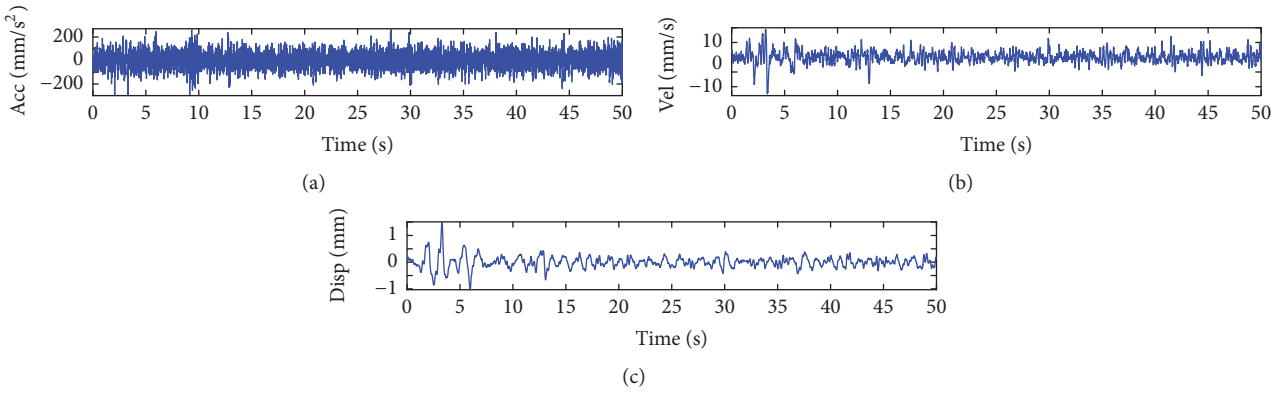

Figure 12: Acceleration integration (right wheel). (a) Acceleration; (b) integral velocity; and (c) integral displacement.

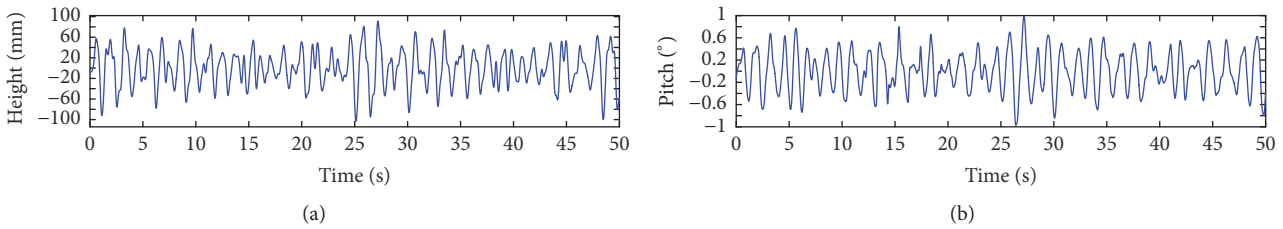

Figure 13: Comparison of low frequency road profile and pitch angle (right wheel). (a) The low frequency road profile; (b) the pitch angle.

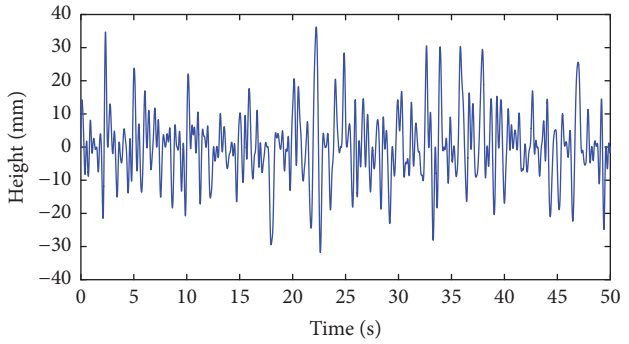

Figure 14: Low frequency road profile after correction (right wheel).

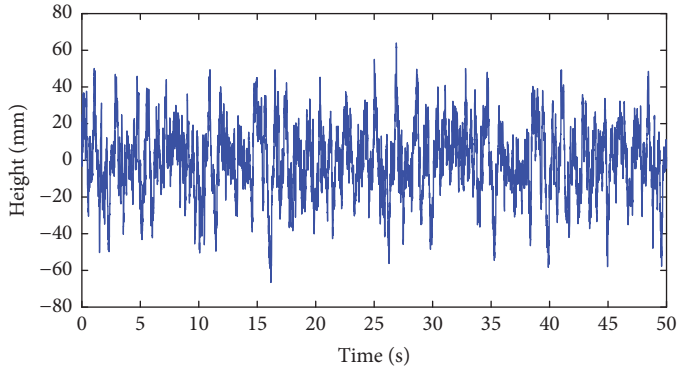

Figure 15: Final corrected road profile (right wheel).

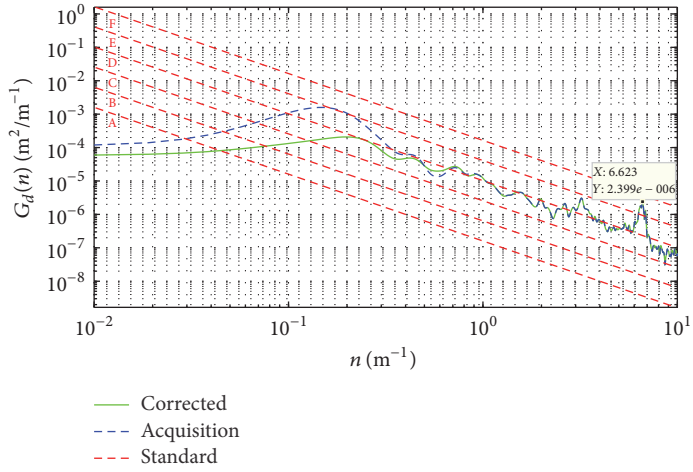

Figure 16: Space PSD of the road profiles $G_d(n)$.

However, the road profile measured in this paper is time domain displacement $D(\tau)$. The time domain road profile $D(\tau)$ should transform into space domain displacement $D(S)$ based on the distance history $S(\tau)$, which is obtained by vehicle speed $v(\tau)$ integration measured by GPS module. Then the space domain spectrum $G_d(n)$ of road profile is calculated through Fast Fourier Transform (FFT) based on $D(S)$, as shown in Figure 16.

In Figure 16, six standard road spectra from Grade A to Grade F according to ISO/DIS 8608 have been plotted as references. The space PSD of corrected and acquisition road profile have also been plotted for comparison. Besides, it is noted that the peak at a space frequency of 6.623 cycles/meter corresponds to the wavelength of about 150 mm which is the average length of the cobbles. It can be concluded that, in the whole interested frequency range, the error correction method raised in the paper shows its advantage by obtaining a more accurate PSD as removing the vehicle vibration and attitudes impacts. The proposed method can adapt various unstructured road profile measuring and correcting and provides accurate road spectra for road simulation test.

5. Conclusions

The acquisition system integrated by laser height sensors, accelerometers, and strapdown gyroscope can be easily mounted and quickly deployed on a testing vehicle to acquire the road profile for road simulation. With the vibration acceleration history and the vehicle's attitude history, respectively, obtained by the accelerometers and strapdown gyroscope, the measured road profiles can be accurately corrected by the frequency division and sliding block overlap calibration method. The validity of the method has been verified by applying to measure and correct the road profile of the Belgian Road.

However, the proposed method is limited by vehicle speed, straight-line driving, long-wave of road, and so forth. Vehicle rapid cornering will affect the accuracy of gyro attitude measurement. The gyro attitudes frequency band and road frequency band of measured road profiles will be difficult to divide due to the improper vehicle speed and long-wave of road. Therefore, the vehicle speed and testing road section should be determined before the testing to improve the applicability of the proposed method.

Though the method proposed in this paper is only verified under the Belgian Road situation, the method is applicable for measuring of other kinds of roads after proper amendments, especially for unstructured roads due to their large range vehicle vibration and attitudes change which are easy to be measured by sensors. Moreover, aided with high precision GPS receiver for low frequency road profile measuring (<0.1 Hz), the method can also be applicable to the road profile measuring and Noise Vibration Harshness (NVH) assessment with wider bandwidth and higher accuracy requirement.

Abbreviations

PSD: Power spectral density
GPS: Global Positioning System
RTK: Real Time Kinematics
GCS: Geographic coordinate system
BCS: Body coordinate system
PG: Proving ground
RMS: Root Mean Square
FFT: Fast Fourier Transform
NVH: Noise Vibration Harshness.

Competing Interests

The authors declare that there is no conflict of interests regarding the publication of this paper.

Acknowledgments

This work is supported by Weapon and Equipment Exploration Research Project (no. 7131255).

References

[1] K. Reza-Kashyzadeh, M. J. Ostad-Ahmad-Ghorabi, and A. Arghavan, "Investigating the effect of road roughness on automotive component," *Engineering Failure Analysis*, vol. 41, no. 3, pp. 96–107, 2014.

[2] P. E. Uys, P. S. Els, and M. Thoresson, "Suspension settings for optimal ride comfort of off-road vehicles travelling on roads with different roughness and speeds," *Journal of Terramechanics*, vol. 44, no. 2, pp. 163–175, 2007.

[3] G. Li and T. Wang, "Influence of long-waved road roughness on fatigue life of dump truck frame," *Journal of Vibroengineering*, vol. 16, no. 8, pp. 3862–3878, 2014.

[4] M. N. Tautan, S. Miclos, D. Savastru, and A. Stoica, "Longitudinal road profile reconstruction from dual laser scans," *Optoelectronics and Advanced Materials, Rapid Communications*, vol. 8, no. 7, pp. 622–625, 2014.

[5] W. R. Graham, F. Liu, M. P. F. Sutcliffe, and M. Dale, "Characterisation and simulation of asphalt road surfaces," *Wear*, vol. 271, no. 5-6, pp. 734–747, 2011.

[6] V. Rouillard, "Statistical models for nonstationary and non-Gaussian road vehicle vibrations," *Engineering Letters*, vol. 17, no. 4, pp. 1–11, 2009.

[7] N. Cong, J. Shang, and Y. Ren, "Unstructured road spectrum α-stable distribution parameters interval estimation and reconstruction based on moving block bootstrap method," *Journal of Mechanical Engineering*, vol. 49, no. 4, pp. 106–113, 2013.

[8] Y. Du, C. Liu, D. Wu, and S. Jiang, "Measurement of international roughness index by using Z-axis accelerometers and GPS," *Mathematical Problems in Engineering*, vol. 2014, Article ID 928980, 10 pages, 2014.

[9] P. Johannesson, K. Podgórski, and I. Rychlik, "Modelling roughness of road profiles on parallel tracks using roughness indicators," *International Journal of Vehicle Design*, vol. 70, no. 2, pp. 1–28, 2016.

[10] D. J. Wilson, B. Jacobsen, and W. Chan, "The effect of road roughness (and test speed) on GripTester measurements," Research Report 523, NZ Transport Agency, Wellington, New Zealand, 2013.

[11] M. Yousefzadeh, S. Azadi, and A. Soltani, "Road profile estimation using neural network algorithm," *Journal of Mechanical Science and Technology*, vol. 24, no. 3, pp. 743–754, 2010.

[12] A. Cigada, F. Mancosu, S. Manzoni, and E. Zappa, "Laser-triangulation device for in-line measurement of road texture at medium and high speed," *Mechanical Systems and Signal Processing*, vol. 24, no. 7, pp. 2225–2234, 2010.

[13] P. Kumar, P. Lewis, C. P. Mcelhinney, and A. A. Rahman, "An algorithm for automated estimation of road roughness from mobile laser scanning data," *Photogrammetric Record*, vol. 30, no. 149, pp. 30–45, 2015.

[14] N. Cong, J. Shang, Y. Ren, and Y. Guo, "Vehicle unpaved road response spectrum acquisition based on accelerometer and GPS data," *Sensors (Switzerland)*, vol. 12, no. 8, pp. 9951–9964, 2012.

[15] M. L. Westphalen, B. L. Steward, and S. Han, "Topographic mapping through measurement of vehicle attitude and elevation," *Transactions of the American Society of Agricultural Engineers*, vol. 47, no. 5, pp. 1841–1849, 2004.

[16] V. Žuraulis, L. Levulyte, and E. Sokolovskij, "The impact of road roughness on the duration of contact between a vehicle wheel and road surface," *Transport*, vol. 29, no. 4, pp. 431–439, 2014.

[17] C. Gohrle, A. Schindler, A. Wagner, and O. Sawodny, "Road profile estimation and preview control for low-bandwidth active suspension systems," *IEEE/ASME Transactions on Mechatronics*, vol. 20, no. 5, pp. 2299–2310, 2014.

[18] A. Farah, "Digital road profile using kinematic GPS," *Artificial Satellites*, vol. 44, no. 3, pp. 95–101, 2010.

[19] C. Mekik and M. Arslanoglu, "Investigation on accuracies of real time kinematic GPS for GIS applications," *Remote Sensing*, vol. 1, no. 1, pp. 22–35, 2009.

[20] B. R. Davis and A. G. Thompson, "Power spectral density of road profiles," *Vehicle System Dynamics*, vol. 35, no. 6, pp. 409–415, 2001.

[21] S. Wang, "Research on laser Gyro strapdown attitude & heading road-spectrum measurement system," Doctor Paper, National University of Defense Technology, Changsha, China, 2006.

[22] T. J. Ulrych, M. D. Sacchi, and J. M. Graul, "Signal and noise separation: art and science," *Geophysics*, vol. 64, no. 5, pp. 1648–1656, 1999.

[23] H. M. Duan, Y. Ma, F. Shi, K. B. Zhang, and F. Xie, "Smooth connection method of segment test data in road surface profile measurement," in *Proceedings of the 4th International Conference on Machine Vision (ICMV '11)*, pp. 8349:1–8349:7, Singapore, 2011.

[24] H.-M. Duan, F. Xie, K.-B. Zhang, Y. Ma, and F. Shi, "Methods of signal pre-processing with massive road surface measurement data," *Journal of Vibration & Shock*, vol. 30, no. 8, pp. 101–117, 2011.